Fluid Phase Equilibria 280 (2009) 16–21

Contents lists available at ScienceDirect

Fluid Phase Equilibria

journal homepage: www.elsevier.com/locate/fluid

A molecular-dynamics study of thermal and physical properties of platinum nanoclusters

Hamed Akbarzadeh, Gholam Abbas Parsafar*,[1]

Department of Chemistry and Nanotechnology Research Center, Sharif University of Technology, Tehran 11365-9516, Iran

ARTICLE INFO

Article history:
Received 7 November 2008
Received in revised form 25 February 2009
Accepted 26 February 2009
Available online 13 March 2009

Keywords:
Molecular-dynamics
Thermal and physical properties
Platinum nanoclusters

ABSTRACT

Metallic nanoclusters are interesting because of their utility in catalysis and sensors. The thermal and physical characteristics of metallic Pt nanoclusters with different sizes were investigated via molecular-dynamics simulations using Quantum Sutton-Chen (QSC) potential. This force field accurately predicts solid and liquid states properties as well as melting of the bulk platinum. Molecular dynamic simulations of Pt nanoclusters with 256, 456, 500, 864, 1372, 2048, 2916, 4000, 5324, 6912, 8788 atoms have been carried out at various temperatures. The Pt-Pt radial distribution function, internal energy, heat capacity, enthalpy, entropy of the nanoclusters were calculated at some temperatures. These properties are used to characterize the physical phase and also to determine the melting transition of each nanocluster. The melting point predicted by the various properties is consistent with each other and shows that the melting temperature increases with the particle size, approaching to the bulk limit for the largest one. The size dependence of the melting point has been reported, both experimentally and theoretically for the atomic nanoclusters. We have found that the melting of the platinum nanoclusters commences at the surface and the relation $T_{m,N} = T_{m,bulk} - \alpha N^{-1/3}$ between the melting point of nanocluster ($T_{m,N}$) and that of the bulk ($T_{m,bulk}$) holds. The extrapolation of $T_{m,N}$ versus $N^{-1/3}$ gives $T_{m,bulk}$ = 2058.1 K which is in a good agreement with the experimental value of 2041 K.

1. Introduction

Particles with diameters of 1–10 nanometer exhibit properties that are often an intermediate between those of the molecular and crystalline states.

A comprehensive set of studies of the physical properties of nanoparticles, too small to be subjected to macroscopic thermodynamic analysis, have been carried out over the past two decades by Berry and co-workers [1–7]. Melting is one of the most studied and best characterized processes for a nanoparticle. In small nanoparticles, the surface and core atoms are not distinct, and liquid and solid phases of the nanoparticle are in dynamic equilibrium rather than in coexistence. Only the solid form is stable for temperatures lower than the fusion temperature and only the liquid form is stable for temperatures higher than the melting point. At temperatures between the fusion temperature and melting temperature the nanoparticle fluctuates between the solid and liquid states, much like the equilibrium between two chemical isomers.

Metal nanoparticles exhibit physical, chemical, and electronic properties different from those of the bulk and single molecules due to the large fraction of surface atoms. Considerable experimental and theoretical researches have been dedicated to understand the thermodynamics [8] and kinetics of nanoparticle growth and stabilization when subjected to a thermal or any other stresses [9–12]. Melting properties of the metal nanoclusters and their associated effect on the shape and composition would have a bearing on the method of synthesis, processing, and the performance of these nanoclusters in various areas of application. The melting point of a nanocluster decreases with decreasing cluster size and its value may be much lower than of the bulk [13–17].

This lowering effect is mainly attributed to the large percentage of weakly bounded surface atoms which are less constrained in their thermal motions. However, there is very little quantitative data on the structure and energy of bulk and surface regions governing the properties of nanoparticle. Computer simulations offer an effective tool to study properties of nanoclusters and complement ongoing experimental efforts [18–20]. A molecular dynamic simulations study of melting, freezing, and coalescence of gold nanoclusters, in the size range of 135–3995 atoms, indicated that melting begins at the surface and proceeds inward the core [21].

Molecular dynamic (MD) studies on melting of Ni nanoclusters up to 8007 atoms indicates that a transition from molecular behavior below 500 atoms to a mesoscale regime above 750 atoms

* Corresponding author. Tel.: +98 21 66165355; fax: +98 21 66005718.
E-mail addresses: hamedakbarzadeh@mehr.sharif.edu (H. Akbarzadeh), parsafar@sharif.edu, parsafar@chem.ubc.ca (G.A. Parsafar).
[1] Temporary address: Department of Chemistry, UBC, Vancouver, BC, Canada.

0378-3812/$ – see front matter © 2009 Elsevier B.V. All rights reserved.
doi:10.1016/j.fluid.2009.02.018

with well defined bulk and surface properties [22]. The final atomic arrangements in Au nanoclusters have been found to be strongly influenced by thermodynamic factors and kinetic growth [23]. Potential energy distribution of transition metal clusters shows the coexistence of a surface melted phase with a solid core for clusters larger than 200 atoms [24]. The phase change was mainly attributed to isomerization transitions, as no premelting peak was detected in the heat capacity curve. A nonmonotonic variation of melting temperature with cluster size is found for very small sized clusters [16]. Experimental studies on tin nanoclusters having 10–30 atoms corroborate this finding [25]. We have used molecular-dynamics (MD) simulations to study solid and liquid properties of Pt nanoclusters with 256–8788 atoms, in which the quantum Sutton-Chen potential was used to investigate the melting point. Therefore our aim is to extend the MD simulations, to investigate the dynamic and thermodynamic properties of platinum, to much larger nanoclusters than those previously studied [26,27]. We have calculated the Pt-Pt radial distribution function, atomic diffusion coefficient, and thermal properties at various temperatures for the nanoclusters. The size dependencies of thermodynamic properties are investigated and their dependencies are examined with the expressions given for Cu nanoclusters. Also, the abrupt change of different thermodynamic properties within the solid–liquid phase transition is used to predict the melting points of the nanoclusters. The predicted values are found to be consistent.

2. Molecular dynamic simulation

2.1. Force field model

In the present study, molecular dynamic simulations on solid and liquid platinum nanoclusters were done using the DL-POLY-2.18 program [28]. All thermodynamic and transport properties were obtained as time averages over the particle positions and velocities. The embedded atom potentials [29] and other long-range potentials like the Sutton-Chen based on [30] the Finnis-Sinclair type of potentials have been used in the literature successfully to produce the properties of FCC based metals such as Pt. Based on the Sutton-Chen potential, the potential energy of a finite system is given by,

$$U_{\text{tot}} = \sum_i U_i = \sum_i \varepsilon \left[\sum_{j \neq i} \frac{1}{2} V(r_{ij}) - c\rho_i^{1/2} \right] \quad (1)$$

where $V(r_{ij})$ is the pair potential to account for the repulsion resulting from the Pauli's exclusion principle,

$$V(r_{ij}) = \left(\frac{a}{r_{ij}} \right)^n \quad (2)$$

The local density accounting for the cohesion associated with atom i is given by,

$$\rho_i = \sum_{j \neq i} \Phi(r_{ij}) = \sum_{j \neq i} \left(\frac{a}{r_{ij}} \right)^m \quad (3)$$

Sutton and Chen restricted the value of m to be greater than 6 and fitted it to give a close agreement with the bulk modulus and elastic constants. The Sutton-Chen potential poorly predicts properties involving defects, surfaces, and interfaces. The quantum Sutton-Chen potential includes the quantum corrections and takes into account the zero-point energy allowing better prediction of temperature dependent properties. The Quantum Sutton-Chen (QSC) parameters for Pt are listed in Table 1 [31].

Table 1
Potential parameters used in MD simulations for Pt nanoclusters.

Sutton-Chen	n	m	ε (eV)	c	a (Å)
QSC	11	7	0.0097894×10^{-3}	34.428	3.92

2.2. MD simulation details

The MD simulations were carried out in an ensemble approximating the canonical with a constant number of atoms N and volume V without any periodic boundary conditions. A constant temperature Evans thermostat [32] was used. The equations of motion were integrated using the Verlet Leapfrog algorithm [18] with a time step of 0.001 ps. The cluster was initially subjected to mild annealing in the 0–300 K interval. This was followed by heating to 2000 K with increments of 100 K. Near the melting point, the temperature increments were reduced to 10 K and 1 K to account for the large temperature fluctuations. The simulations were carried out for 400 ps of equilibrium followed by production time of 200 ps for generating the time average properties. All interatomic interactions were determined for the atoms in the simulation within a cutoff distance of R_{cutoff}. Platinum is a metal with a FCC structure. A FCC block was first constructed from a FCC unit cell by replication in the *abc* directions with center located at (0, 0, 0). The cluster cutoff radius is defined as [33],

$$R_c = R_g \sqrt{\frac{5}{3}} + R_i \quad (4)$$

where the interatomic radius for the Pt system, R_i = 1.39 Å, and the radius of gyration R_g is given by,

$$R_g^2 = \left(\frac{1}{N} \right) \sum (R_i - R_{c,m})^2 \quad (5)$$

where $(R_i - R_{c,m.})$ is the distance of atom i from the cluster center of mass. To analyze how the atomic motions change near the melting point, we partitioned the cluster into six radial shells of equal dR within each shell to calculate the average root-mean-square thermal displacement (RMSD) as,

$$\text{RMSD}_{\text{shell}}(\text{d}t) = \frac{\sqrt{\left(\sum_{t=0}^{t-\text{d}t} (r_i(t+\text{d}t) - r_i(t))^2\right)}}{N_{\text{shell}}} \quad (6)$$

To obtain RMSD, we averaged over a 400 ps trajectory and used dt as 10 ps, which is a sufficiently long time for diffusion in the liquid phase. The dramatical change of RMSD upon melting indicates the first order transition.

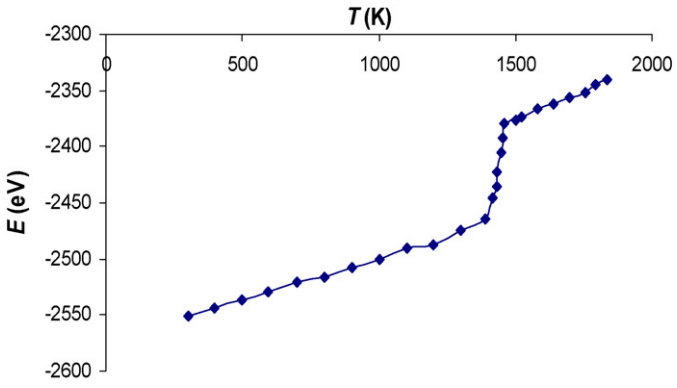

Fig. 1. Potential energy variation with temperature for a Pt nanocluster with 456 atoms.

Table 2
The range of melting temperatures (K) determined from potential energy versus temperature for the Pt nanoclusters with various number of atoms.

Cluster size	Melting range
256	1281–1317
456	1410–1435
500	1450–1468
864	1553–1567
1372	1622–1632
2048	1676–1684
2916	1718–1724
4000	1758–1763
5324	1779–1784
6912	1799–1802
8788	1829–1830

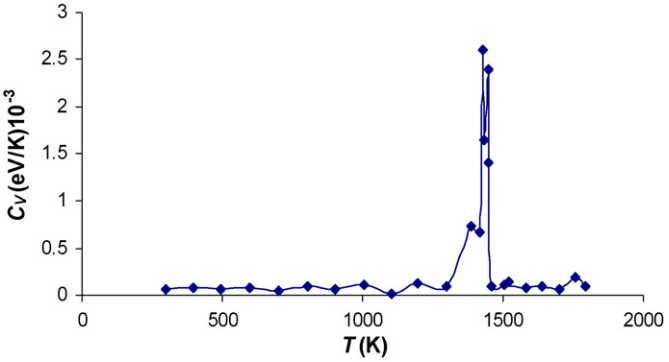

Fig. 2. Variation of specific heat capacity at constant volume with temperature for a Pt nanocluster with 456 atoms.

3. Results and discussion

The transition temperature from the solid to liquid phase and vice versa is usually identified by studying the variation in thermodynamic properties such as potential energy, specific heat capacity, or some other physical properties.

3.1. Melting point determination from potential energy

The force field has been used to calculate the melting point in nanoclusters with generally quite good agreement with experimental results. The predicted melting point of 2070 K, obtained in this simulation, is in a good agreement with the experimental value of 2041 K for the bulk Pt. For simulation of the bulk system, we have set the periodic boundary condition. Fig. 1 shows the temperature dependence of the potential energy of a Pt nanocluster, with 456 atoms.

The phase transition from solid phase to liquid phase and vice versa can be identified by a simple jump in the total potential energy curve. The temperature jump for this naocluster occurs within 1410–1435 K. Similar calculations were carried out to find the temperature range of the melting, for other nanoclusters. The result for various nanoclusters is given in Table 2.

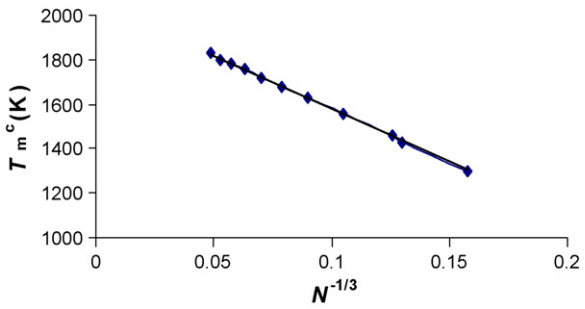

Fig. 3. Dependence of melting temperature on the cluster size.

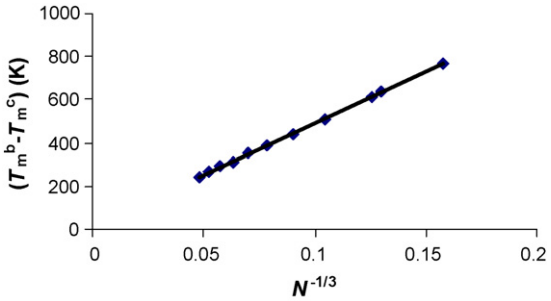

Fig. 4. $T_m^b - T_m^c$ as a function of $N^{-1/3}$.

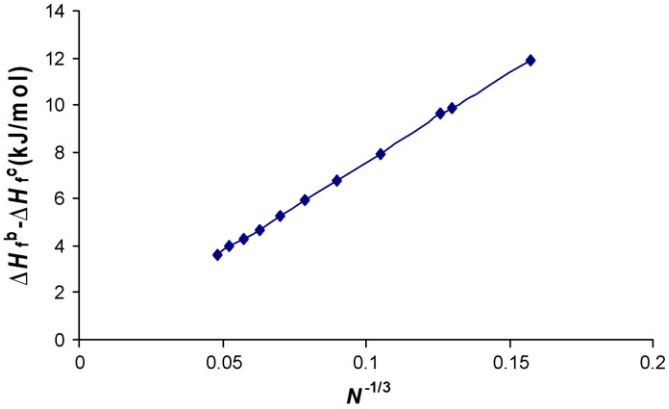

Fig. 5. $\Delta H_f^b - \Delta H_f^c$ as a function of $N^{-1/3}$.

3.2. Melting point determination from heat capacity

Conventionally, two different statistical methods are employed to calculate the heat capacity. The first method derives the heat capacity from the fluctuation of the internal energy, i.e., [34]

$$C_v = \frac{\langle \delta E^2 \rangle_{NVT}}{kT^2} \quad (7)$$

where k is the Boltzmann factor. While, the second method determines the heat capacity from the differential of internal energy with

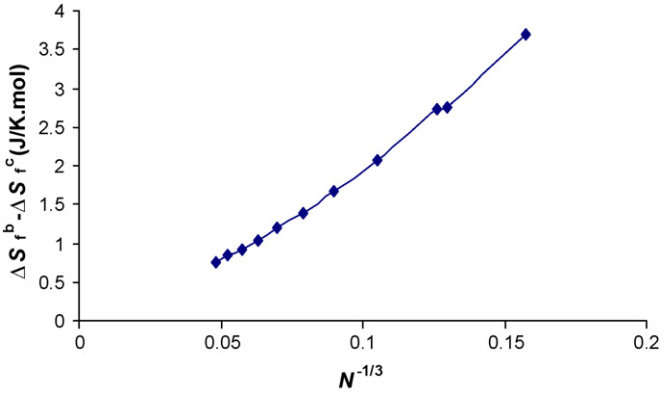

Fig. 6. $\Delta S_f^b - \Delta S_f^c$ as a function of $N^{-1/3}$.

Table 3
Thermodynamic properties obtained from the MD for various clusters as a function of size and the number of atoms within the cluster.

Cluster size (N)	Melting point (K)	ΔH_f (kJ/mol)	ΔS_f (J/K mol)
256	1300.00	7.19	5.53
456	1430.00	9.27	6.48
500	1460.00	9.50	6.50
864	1560.00	11.16	7.15
1372	1630.00	12.30	7.54
2048	1680.00	13.15	7.82
2916	1720.00	13.80	8.02
4000	1760.00	14.40	8.18
5324	1780.00	14.80	8.31
6912	1800.00	15.10	8.38
8788	1830.00	15.80	8.46
Extrapolation	2058.10	19.15	9.84
Bulk (simulation)	2070.00	19.10	9.22
Bulk (experiment)	2041.00	20.00	9.79

Table 4
Radius at 300 K and at the melting point temperature, along with the surface energy for the given platinum nanoclusters.

Cluster size	Cluster radius (at 300 K) (Å)	Cluster radius (at melting point) (Å)	Surface energy (J m^{-2})
256	9.94	9.96	9.79
456	12.05	12.07	9.81
500	12.43	12.45	9.87
864	14.91	14.94	9.91
1372	17.40	17.43	9.94
2048	19.88	19.92	9.98
2916	22.37	22.41	10.00
4000	24.86	24.90	10.03
5324	27.34	27.39	10.04
6912	29.83	29.88	10.10
8788	32.31	32.37	10.23

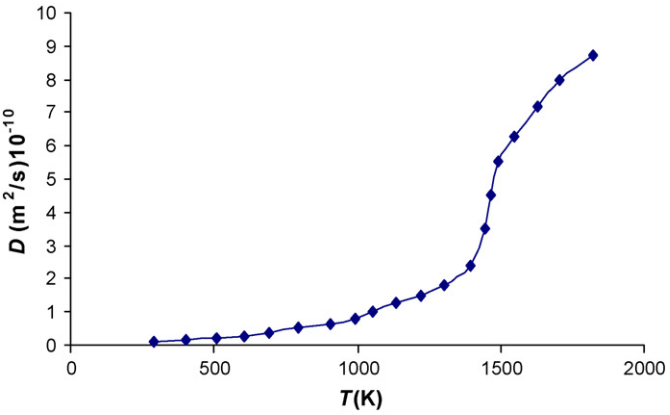

Fig. 7. Variation of self-diffusion coefficient with temperature for a Pt nanocluster with 456 atoms.

respect to temperature, i.e.

$$C_v = \frac{dE(T)}{dT} \tag{8}$$

To identify the melting temperature, the calculated specific heat capacity at constant volume using Eq. (7) is plotted versus temperature in Fig. 2 for a nanocluster with 456 Pt atoms. The maximum in the specific heat capacity corresponds to the temperature jump in potential energy of Fig. 1. Similar calculation was done for the other nanoclusters, to obtain their melting point temperatures. To see the size dependence of the melting point, the calculated values are plotted in Fig. 3 versus $N^{-1/3}$.The data fits well into a line with the coefficient of determination of $R^2 = 0.9986$. The extrapolation of the line to $N = \infty$ gives $T_m = 2058.1$ K, compare to experimental value of 2041 K for Pt bulk.

Also the calculated melting points for the 11 different Pt nanoclusters along with the calculated bulk melting point of Pt, 2070 K, were used to plot $T_m^b - T_m^c$ versus $N^{-1/3}$, shown in Fig. 4, which

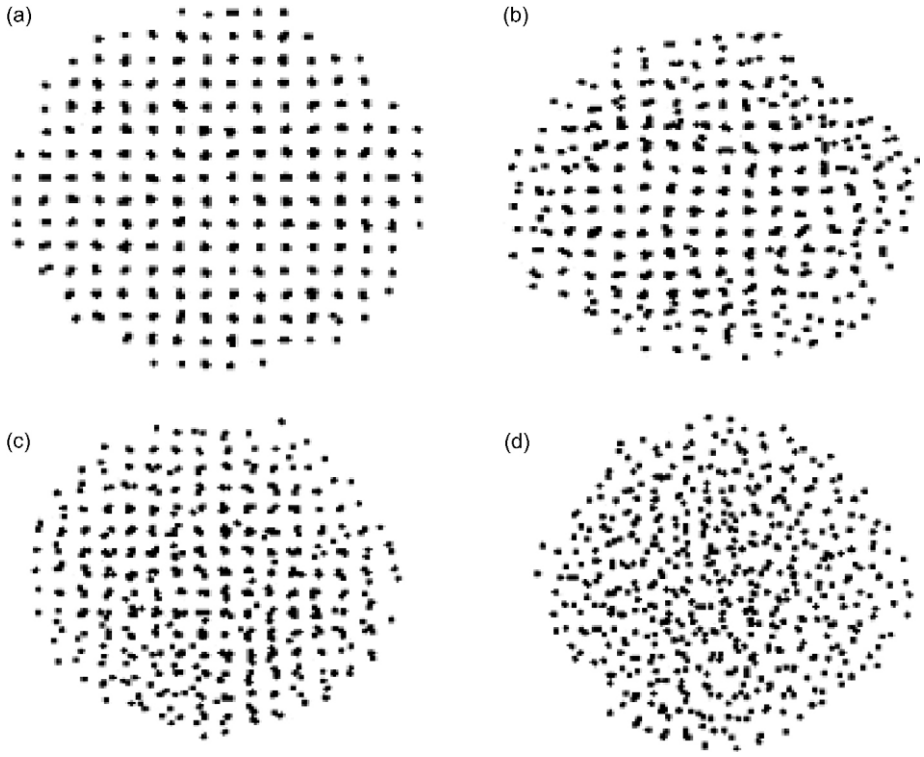

Fig. 8. Snapshot of a nanocluster of platinum with 1063 atoms at (a) 300, (b) 1500, (c) 1600, and (d) 1700 K, respectively.

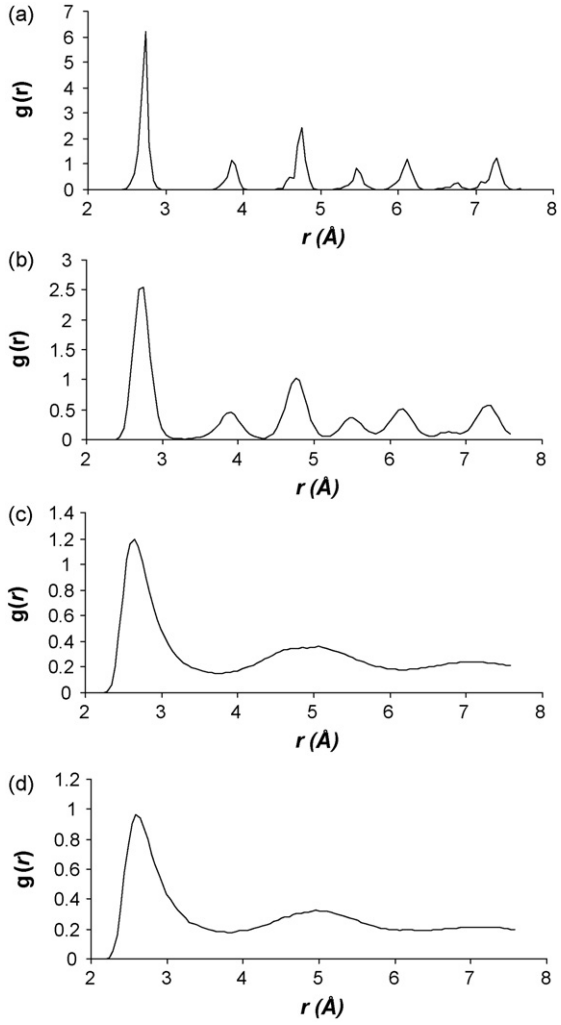

Fig. 9. The Pt-Pt radial distribution function, $g_{\text{Pt-Pt}}$ for a nanocluster with 256 atoms at (a) 10 K, b) 300 K, (c) 1300 K, and (d) 1900 K.

shows a good linearity with the coefficient of determination of $R^2 = 0.998$.

3.3. Fusion enthalpy and entropy

Since the volume of the system is a finite value and pressure is adjusted such that to maintain at zero value, the enthalpy of the system is equal to its potential energy. In order to obtain the heat of fusion of a cluster at its melting point (ΔH_m), the potential energy is fitted into a second order function of temperature, both for the liquid (H_l^c) and solid (H_x^c) states. The heat of fusion at any particular temperature is given by the potential energy difference ($H_f^c = H_l^c - H_x^c$). Mean while, the heat of fusion of the bulk system is calculated from $H_f^b = H_l^b - H_x^b$, where H_l^b and H_x^b denote the potential energy in the liquid and solid states, respectively [33]. The entropy change for the phase transition can be simply calculated from $\Delta S_f = \Delta H_f/T$ at any given temperature. Assuming that the core part of a cluster has the same heat of fusion as the bulk phase, the enthalpy of a cluster in the solid and liquid states may be given as,

$$H_{\text{solid}}^{\text{cluster}} = H_x^c - \gamma_x A \tag{9}$$

$$H_{\text{liquid}}^{\text{cluster}} = H_l^c - \gamma_l A \tag{10}$$

where A is surface area of the cluster and γ_x and γ_i are its surface energy per unit area in the solid and liquid states, respectively. Note that the difference in the enthalpies is due to higher energy of molecules on the surface of cluster, compare to those in the bulk. The extra energy is given by the second term on the right side of Eqs. (9) and (10) for solid and liquid, respectively. To obtain the average fusion energy per molecule, we may subtract Eq. (9) from Eq. (10), and then divide the result by N. If we take into account that A is proportional to $N^{2/3}$, the final result can be found as [33]. Therefore, the heat of fusion for a Pt nanocluster scales linearly with $N^{-1/3}$, i.e.,

$$\Delta H_f^b - \Delta H_f^c(N) = aN^{-1/3} \tag{11}$$

where a is the proportionality constant. The quantity on the left side of Eq. (11) is calculated for the 11 different Pt nanoclusters. The calculated results are plotted in Fig. 5, which shows a good linearity with the coefficient of determination $R^2 = 0.989$. When the cluster size increases, the fusion enthalpy increases and approaches to experimental value.

Almost a similar linearity was found for the calculated fusion entropies, shown in Fig. 6, for ΔS versus $N^{-1/3}$.

The calculated thermodynamic properties for the nanoclusters are summarized in Table 3, including the melting temperature obtained from heat capacity curve, fusion enthalpy, and fusion entropy. Also, the extrapolated and simulated values for the bulk are included.

3.4. Surface energy

The surface energy of a cluster may be calculated from [33]

$$\gamma = \frac{P_{\text{E cluster}} - P_{\text{E Bulk}}}{4\pi {R_C}^2} \tag{12}$$

where $P_{\text{E cluster}}$ and $P_{\text{E Bulk}}$ are the potential energies of the cluster and bulk Pt, respectively, at a certain temperature. We have calculated the surface energy (per unit surface area) and cluster radius, at both 300 K and melting point temperature for the nanoclusters. The results are given in Table 4. As shown in this table, the surface energy gradually increases with the cluster size, from 9.79 to 10.23 J/m^2 for nanoclustes with 256 and 8788 atoms, respectively.

3.5. Self-diffusion coefficient

The self-diffusion coefficient can be obtained either from the positions or velocities of molecules. The mean square displacement (MSD) is proportional to observation time for the infinite time limit. The proportionality constant relating the MSD to the observation time is known as the self-diffusivity, D, which is given by

$$D \equiv \frac{1}{2d} \lim_{t\to\infty} \frac{\left\langle [r(t_0 + t) - r(t)]^2 \right\rangle}{t} \tag{13}$$

where d is the dimensionality of the system and $r(t)$ refers to the vector position of the molecule at time t. The ensemble average is taken over all molecules in the system and over several time origins [35]. A linear least square regression is performed on the MSD curve to find the slope ($2dD$) from which the diffusivity at any temperature can be obtained. Fig. 7 shows the variation of the calculated self-diffusion coefficient of the Pt nanocluster with 456 atoms with temperature. At the melting point, however, the diffusivity of the nanocluster shows a sharp increase, which is an indication for the first order transition. In the liquid phase, the diffusion coefficient shows a noticeable increment with temperature, compare to the solid phase.

3.6. Physical state from molecular point of view

A snapshot for a nanocluster with 1372 Pt atoms at 300, 1500, 1600, and 1700 K is shown in Fig. 8(a)–(d), respectively. The snapshots provide a clear evidence for the increasing of thickness of the

liquid skin over the cluster surface at 1500 and 1600 K and show that the cluster is in the molten state at 1700 K. The performed simulations were used to calculate the physical properties of the nanoclusters, both in the solid and liquid states. However, the structure of the solid and liquid phases may also be characterized at various temperatures by the Pt-Pt radial distribution function,

$$g_{\mathrm{Pt-Pt}}(r) = \frac{1}{nN}\left\langle \sum_i \sum_j \delta\left[r - r_{ij}\right]\right\rangle \quad (14)$$

where N is the total number of Pt atoms, n is number density, and r_{ij} is the distance between i and j atoms; and the brackets indicate the ensemble average. The retention of crystallographic structure in a nanocluster can be quantitatively characterized by the Pt-Pt radial distribution function. The radial distribution function for a Pt nanocluster with 256 atoms is shown at four different temperatures in Fig. 9. Note that the scaling of the y-axes is different for the figures.

The long-range correlations in the solid phase are obvious from too many peaks appear in $g_{\mathrm{Pt\text{-}Pt}}(r)$ at temperatures 10 and 300 K. As the temperature increases, the vibrational motion of the Pt atoms broadens the peaks in the $g_{\mathrm{Pt\text{-}Pt}}$ curve, compare Fig. 9(c) with Fig. 9(a) and (b). The locations of the peaks, which correspond to the average separation of the atoms, do not change in Fig. 9(a) and (b), indicating a fix position for each atom in the nanocrystal structure, which is expected as far as the anharmonicity is ignored. However, for the liquid phase, shown in Fig. 9(c) and (d), the long-range correlations are lost and also the positions of the maxima, which represent the locations of the neighboring correlation shells, are shifted to longer distances, in comparison with those for the solid.

4. Conclusion

Using MD simulations with the QSC potential, we have studied the melting and the physical properties of Pt nanoclusters and found that the melting temperature and heat of fusion vary linearly with $N^{-1/3}$ for 11 Pt nanoclusters investigated. Melting proceeds from the surface and after liquefaction of the outer shells, melting of the whole clusters begins from the outer shells to core region.

The molar enthalpy, entropy and the surface energy of a cluster increases with its size. The melting point of a nanocluster is clearly identified by studying the variation in either potential energy or specific heat capacity with temperature. The calculated melting points for the nanoclusters are found to be much lower than that of the bulk, see Table 3. On the whole, the description of the melting transition agrees qualitatively with the previous simulation and experimental studies on Cu nanoclusters [33]. Melting of a nanocluster occurs over a temperature range, rather than at a single temperature, in which the range becomes smaller for larger cluster size, see Table 2. Within the melting, the long-range structural feature of a nanocluster, which is related to the long-range ordering, begins to disappear, while short-range structure is retained, see Fig. 9(a)–(d).

References

[1] Calvo, J. Phys. Chem. B 105 (2001) 2183.
[2] R.S. Berry, J. Jellinek, G. Natanson, Phys. Rev. A 30 (1984) 919.
[3] T.L. Beck, J. Jellinek, R.S. Berry, J. Chem. Phys. 87 (1987) 545.
[4] R. Kunz, R.S. Berry, Phys. Rev. E 49 (1994) 1895.
[5] D.J. Wales, R.S. Berry, Phys. Rev. Lett. 73 (1994) 2875.
[6] K.D. Ball, R.S. Berry, R.E. Kunz, F.Y. Li, A. Proykova, D.J. Wales, Science 271 (1996) 963.
[7] A. Proykova, S. Pisov, R. Radev, P. Mihailov, I. Daykov, R.S. Berry, Vacuum 68 (2003) 87.
[8] J.P. Borel, Surf. Sci. 106 (1981) 1.
[9] Z.L. Wang, J.M. Petroski, T.C. Green, M.A. El-Sayed, J. Phys. Chem. B 102 (1998) 6145.
[10] R. Kusche, Th. Hippler, M. Schmidt, B.Von. Issendorff, H. Haberland, Eur. Phys. J. D 9 (1999) 1.
[11] M. Schmidt, R. Kusche, W. Kronmuller, B.Von. Issendorff, H. Haberland, Phys. Rev. Lett. 79 (1997) 99.
[12] J.M. Petroski, Z.L. Wang, T.S. Green, M.A. El-Sayed, J. Phys. Chem. B 102 (1998) 3316.
[13] Ph. Buffat, J.P. Borel, Phys. Rev. A 13 (1976) 2287.
[14] F. Ercolessi, W. Andreoni, E. Tosatti, Phys. Rev. Lett. 66 (1991) 911.
[15] C.L. Cleveland, W.D. Luedtke, U. Landman, Phys. Rev. Lett. 81 (1998) 2036.
[16] F. Calvo, F.J. Spiegelmann, J. Chem. Phys. 112 (2000) 2888.
[17] H. Lei, J. Phys.: Condens. Matter 13 (2001) 3023.
[18] M.P. Allen, D.J. Tildesley, Simulation of Liquids, Oxford University Press, London, 1987.
[19] F. Baletto, C. Mottet, R. Ferrando, Phys. Rev. Lett. 90 (2003) 135504.
[20] V. Walter, Metal Clusters (1999) Wiley Series in Theoretical Chemistry, Wiley, New York, 1999.
[21] L.J. Lewis, P. Jensen, J.L. Barrat, Phys. Rev. B 56 (1997) 2248.
[22] Y. Qi, T. Cagin, W.L. Johnson, W.A. Goddard III, J. Chem. Phys. 115 (2001) 385.
[23] Y.J. Chushak, L.S. Bartell, J. Phys. Chem. B 105 (2001) 11605.
[24] Y.J. Lee, E.K. Lee, S. Kim, R.M. Nieminen, Phys. Rev. Lett. 86 (2001) 999.
[25] A.A. Shvartsburg, M.F. Jarrold, Phys. Rev. Lett. 85 (2000) 2530.
[26] S.H. Lee, S.S. Han, J.K. Kang, H.M. Lee, Mater. Sci. Forum 539 (2007) 3546.
[27] S.H. Lee, S.S. Han, J.K. Kang, J.H. Rya, H.M. Lee, Surf. Sci. 602 (2008) 1433.
[28] W. Smith, I.T. Todorov, Mol. Simulation 32 (2006) 935–943.
[29] S.M. Foiles, M.I. Baskes, M.S. Daw, Phys. Rev. B 33 (1986) 7983.
[30] A.P. Sutton, J. Chen, Philos. Mag. Lett. 61 (1990) 139.
[31] Y. Qi, T. Cagin, Y. Kimura, W.A. Goddard III, Phys. Rev. B 59 (1999) 3527.
[32] D.J. Evans, G.P. Morriss, Comput. Phys. Rep. 1 (1984) 297.
[33] L. Wang, Y. Zhang, X. Bian, Y. Chen, Phys. Lett. A 310 (2003) 197.
[34] M.P. Allen, D.J. Tildesley, Computer Simulation of Liquids, 1st edn, Oxford, New York, 1989, p. 51.
[35] J.M. Haile, Molecular Dynamics Simulations Elementary Methods, John Wiley and Sons, New York, 1992.